NASA CONTRACTOR REPORT

NASA CR-2237

NASA CR-2237

THE VISC CODE - A USER'S MANUAL

by Ken Wilson

Prepared by
LOCKHEED MISSILES & SPACE COMPANY
Sunnyvale, Calif.
for Ames Research Center

NATIONAL AERONAUTICS AND SPACE ADMINISTRATION • WASHINGTON, D. C. • MARCH 1973

1. Report No.	2. Government Accession No.	3. Recipient's Catalog No.
NASA CR-2237		

4. Title and Subtitle	5. Report Date
"The VISC Code--A User's Manual"	March 1973
	6. Performing Organization Code

7. Author(s)	8. Performing Organization Report No.
Ken Wilson	
	10. Work Unit No.

9. Performing Organization Name and Address	11. Contract or Grant No.
Lockheed Missiles & Space Company Sunnyvale, California	NAS 2-6668
	13. Type of Report and Period Covered

12. Sponsoring Agency Name and Address	13. Type of Report and Period Covered
National Aeronautics & Space Administration Washington, D.C.	Contractor Report
	14. Sponsoring Agency Code

15. Supplementary Notes

16. Abstract

The VISC code is a computer automated scheme for solving the equations describing the fully coupled viscous, radiating flow at the stagnation-point of a blunt body which may or may not be ablating. The code provides a basis for obtaining predictions of the stagnation-point heating to a body entering any planetary atmosphere at hyperbolic velocities. The code is written in Fortran V and is operational on both the UNIVAC 1108 (EXEC 8) system in use at LMSC and the CDC 7600 system in use at the University of California, Berkeley. This report gives an overview of the VISC code computational logic flow, a description of the input requirements and output results and comments on the practical use of the code. As such this report forms a "users manual" for operation of the VISC code.

17. Key Words (Suggested by Author(s))	18. Distribution Statement
Stagnation, Viscous, Radiation Ablation, Boundary layer, Entry, Planetary, Heating	UNCLASSIFIED - UNLIMITED

19. Security Classif. (of this report)	20. Security Classif. (of this page)	21. No. of Pages	22. Price*
UNCLASSIFIED	UNCLASSIFIED	38	$3.00

* For sale by the National Technical Information Service, Springfield, Virginia 22151

Page Intentionally Left Blank

ABSTRACT

The VISC code is a computer automated scheme for solving the equations describing the viscous, radiating flow at the stagnation-point of a blunt body which may or may not be ablating. The code provides a basis for obtaining predictions of the stagnation-point heating to a body entering a planetary atmosphere at hyperbolic velocities. The code is written in Fortran V and is operational on both the UNIVAC 1108 (EXEC 8) system in use at LMSC and the CDC 7600 system in use at the University of California, Berkeley. This report gives an overview of the VISC code computational logic flow, a description of the input requirements and output results and comments on the practical use of the code. As such this report forms a "users manual" for operation of the VISC code.

CONTENTS

1. INTRODUCTION

The Lockheed Missile and Space Company's VISC code is a computer implemented computational scheme which provides theoretical predictions of the radiative and convective energy transfer to the stagnation-point of a blunt body during hypervelocity entry into planetary atmospheres. Although prediction of the convective heating rate is a direct consequence of the solution method, the VISC code was developed primarily to analyze those entry conditions where radiative processes dominate the total energy transport. The surface heating rate prediction results from a solution of the coupled equations describing the flow of a viscous, radiating gas at the stagnation point of a blunt body which may or may not be undergoing massive ablation. In developing the code, the objective was always to provide quantitatively meaningful heating predictions as opposed to identifying qualitatively significant phenomena. Accordingly, a serious attempt was made to provide realistic models of the dominant physical processes, especially as regards the spectral nature of the radiative transport processes.

Historically, the VISC code is the result of an eight-year period of development with each subsequent effort providing an increasingly sophisticated accounting of the gasdynamic and transport processes. LMSC's first effort analyzed the relatively simple problem of an inviscid radiating flow in the optically thin approximation.[1] This first effort used an integral method to solve the flow equations and the analysis applied away from the stagnation-point. The second effort continued the methodology previously developed but extended the equations to include viscous effects.[2] The third effort provided a major step forward in complexity by dropping the assumption of an optically thin shock layer and accounted for the spectral behavior of the continuum absorption and emission radiative processes.[3] In addition at this point, a finite-difference solution to the energy equation and inclusion of surface blowing (under a simple

chemistry model) were added. The analysis, however, was still applicable away from the stagnation-point.

The fourth effort considered for the first time the very complex equilibrium chemistry which results from injection of realistic ablation products (e.g., carbon phenolic) into the air shock layer.[4] This realistic treatment of the shock layer chemistry required implementation of the FEMP program into the analysis. The use of FEMP, along with an even more detailed accounting of the spectral radiative transport, raised a computational cost barrier which has since prevented the application of the direct finite-difference analysis away from the stagnation-point. Since this fourth stage, then, the analysis underlying the VISC code has restricted the results to stagnation-point values. Contemporary with the fourth level of effort was realization of the importance of radiative transport in atomic lines and the development of a methodology for line transport.[5]

The fifth level of effort extended the radiative transport analysis to include line transport. Also, with respect to the gasdynamic analysis, a major improvement was the replacement of the integral method of solution of the momentum and diffusion equations by a finite-difference calculation. This placed all three conservation equations on the same footing and permitted analysis of "massive" blowing problems.[6] Recent steps in the development of the VISC code continued the improvement of both the continuum and line radiative transport models and its application to the Jovian entry problem.[7,8] Finally, the simplifying but nonessential gasdynamic approximations that $\rho\mu$ = constant and the construction of an inner inviscid layer near the wall were removed. Hence, the latest results obtained* removed all gasdynamic approximations. These results are from a solution which used a completely variable $\rho\mu$ as well as a technique for integrating the conservation equations toward both the shock and

*We refer specifically to the results given in an unpublished paper: K. Wilson, H. Woodward, M. Tauber and W. Page, "Jupiter Probe Heating Rates," presented at the Symposium on Hypervelocity Radiating Flow Fields for Planetary Entry, Jet Propulsion Laboratory, Pasadena, California, January 14-15, 1972

wall from the interior shock layer point where the stream function passes through zero.[9]

Under the current effort, the radiative transport subroutine was further extended to include wall emission/reflection terms. At this time we dropped the previously employed analytic method[7] for obtaining the flux divergence due to lines and replaced that method with direct numerical differencing of the line flux.

The code has been used to obtain heating predictions for reentry into the earth's atmosphere and for probe entry into the atmosphere of Jupiter and Venus. Within the context of its application by a knowledgeable user, the code is operational on the UNIVAC 1108 (EXEC 8) system in use at LMSC and the CDC 7600 system in use at the University of California, Berkeley.

2. MATHEMATICAL MODEL

The analysis starts with the equations describing a viscous, radiating flow and effects the simplifying assumptions:

- thin layer approximation of the y-momentum equations
- shockwave concentric to body
- collision transport properties appropriate to a binary mixture
- one-dimensional radiative transport
- restriction to an axisymmetric stagnation-point

The resulting differential equations are available in numerous publications. The particular form that has been implemented in our VISC code are derived in detail in the Appendix to Reference 8. The three conservation equations all have the general form

$$\frac{dZ}{d\eta} + PZ + Q = 0$$

where η is a density stretched normal coordinate with the values $\eta = 0$ at wall and $\eta = 1.0$ at the shockwave.

$Z = \rho\mu \frac{df}{d\eta}$ for momentum conservation

$Z = \rho^2 D \frac{dc}{d\eta}$ for species conservation

$Z = \frac{\rho\mu}{Pr} \frac{dg}{d\eta}$ for energy conservation

The quantity f is the tangential velocity normalized to the value immediately behind the shock. The quantity c is the blown gas mass fraction. The quantity g is the total enthalpy* normalized to free stream total enthalpy.

*For the stagnation-point problem of interest the static enthalpy equals the total enthalpy (to order density ratio squared) and we will simply call g the enthalpy.

In general the coefficients P and Q are functions of both the independent variable η as well af f, c or g . Our solution method uses a current guess (f^i, c^i or g^i) on the dependent variable to linearize the basic differential equation. A new value (f^{i+1}, c^{i+1} or g^{i+1}) then is obtained by direct quadrature. The boundary conditions are built-in into the quadrature solutions. Thus this method avoids the computational difficulties associated with the often used technique of solving split boundary condition problems by guessing the function and its derivative at one boundary and forward integrating toward the other boundary.

For a nonblowing problem, the boundary conditions are the known values of f, c and g at the wall and shock. For a blowing problem, the value of the η coordinate at which the stream function passes through zero ($\eta = \eta^*$) is determined from the current estimate on the velocity profile f^i. Chou[9] has shown how the boundary conditions at the wall and shock can be combined through a condition which matches magnitude and slope of the dependent variables to yield boundary conditions at $\eta = \eta^*$. Then a blowing problem offers no more difficulty than a nonblowing case regardless of the level of blowing.

3. COMPUTATIONAL STRUCTURE

A chart is given in Fig. 1 which shows the logic sequence followed in obtaining an iterative solution to the conservation equations. Details on the input/output quantities will be given in the next section. The first step in the VISC code computation is the determination of the properties behind a normal shockwave propagating at the vehicle velocity into the ambient atmosphere. The strong shock approximation is invoked in which the velocity behind the shock is set to zero. This fixes the post shock enthalpy and permits estimation of the post shock pressure to within $(1-\epsilon)$ where ϵ is the density ratio across the shock. A simple iteration using the FEMP subroutine to calculate the actual post shock density leads rapidly to a determination of all shock properties.

The sequential solution of the conservation equations is now initiated. The input estimates of the velocity, blown gas mass fraction and enthalpy provide the data required to start the iteration process. The first step in the iterative cycle is to calculate collisional transport properties. This is accomplished using the FEMP package set of subroutines. Along with the enthalpy and elemental mass fractions (as deduced from the local value of the blown gas mass fraction), the FEMP rountine requires a value for the pressure. This value is taken as a constant equal to that behind the normal shock as calculated above. From FEMP, the variation in temperature, density, viscosity and binary diffusion coefficient across the shock layer is obtained. These properties provide the data required to perform a solution to the momentum equation using the technique discussed in Section 2. Convergence of the velocity profile is obtained via a local iterative loop. For a fixed set of density and diffusion coefficient data together with the just-calculated velocity distribution, it is possible to determine numerically a solution to the diffusion equation without iteration.

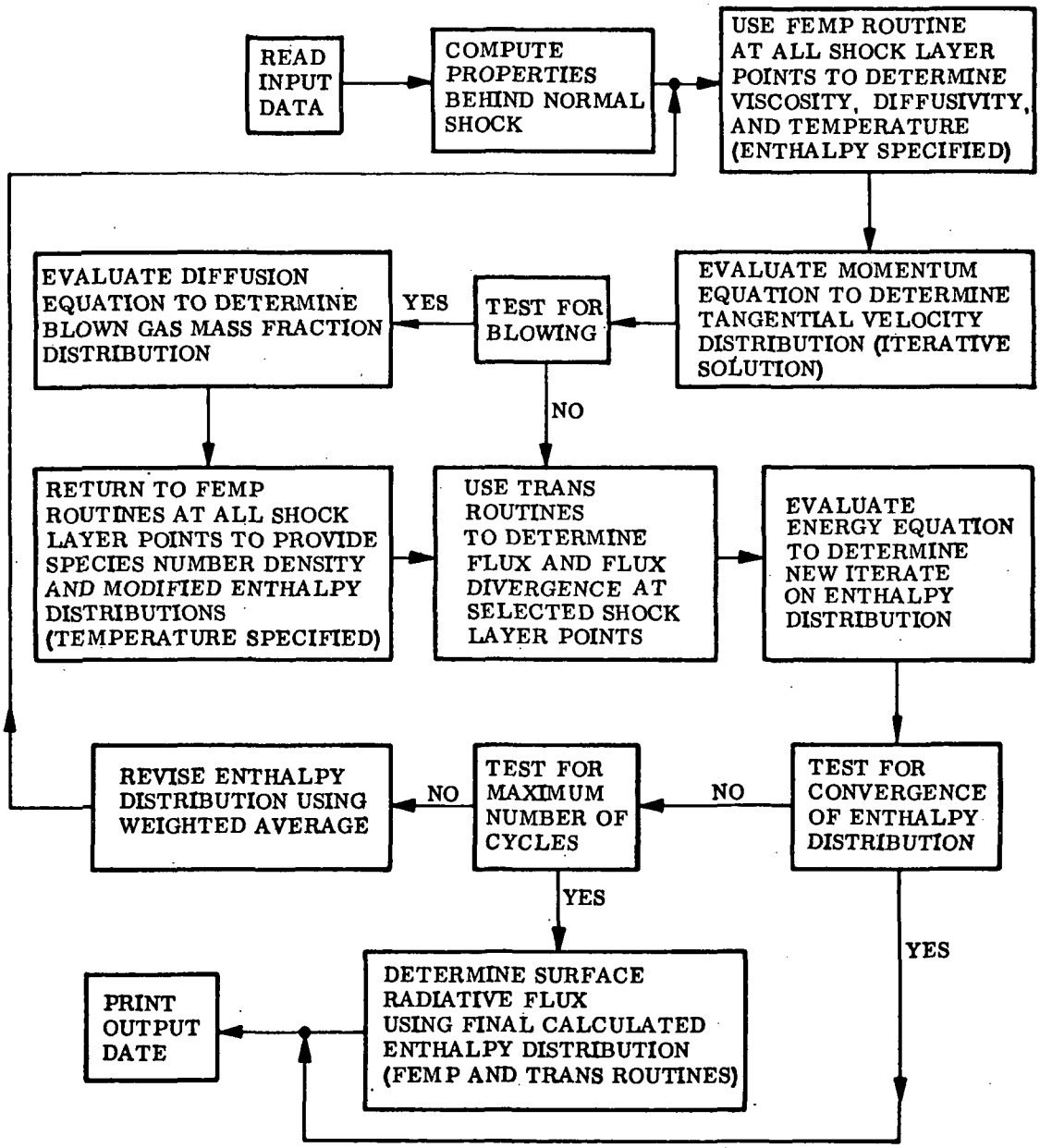

Fig. 1 - Computational Logic Flow

At this point our procedure elects to update the species number density distribution to reflect the change in the blown gas mass fraction profile. It is essential to recognize that in flows dominated by radiative transport effects, temperature is a crucial variable. Indeed, the temperature which is calculated in FEMP from the input enthalpy-mass fraction distribution must be a "reasonable" distribution. Having established a reasonable temperature distribution from the initial guess it is imperative to the stability of the solution to prevent the initial temperature profile from being altered to a large degree in a single step. Such a large temperature change often will occur if we hold the enthalpy at its initial value and calculate a new temperature, density and species number density profile using the updated elemental mass fraction distribution. The reason which underlies the temperature change problem is the following. For flows dominated by radiative transport and especially at high Reynolds numbers, the shear layer is nearly isothermal. However, a rapid change in elemental mass fraction occurs across the shear layer. Since the effective heat capacity of the blown gas may be quite different than that of the atmospheric gas, then the rapid change in the elemental mass fractions is accompanied by rapid change in the enthalpy despite the nearly isothermal character of the shear layer. Hence, if in the updating of the elemental mass fractions, the injected gas moves to a point where the enthalpy is significantly different, the resultant temperature is physically unrealistic and causes catastrophic failure of the energy equation.

To eliminate this high sensitivity between the diffusion and energy equations, our approach fixes temperature at the current value obtained on the first pass through FEMP. Thus in the second pass through FEMP, the temperature is the independent thermodynamic variable and updated values of enthalpy, density and species number density are determined. Of course, for a nonblowing there is no requirement to solve the diffusion equation, and similarly, no requirement for a second pass through FEMP. Thus, for a nonblowing problem, these two stages are bypassed as indicated in Fig. 1

Having updated the species number densities and using the current

temperature profile, the next step is to determine the radiative flux divergence across the shock layer. In deriving the equations describing the radiative transport across the shock layer, it was convenient to use the physical shock layer normal coordinate. Accordingly, the first task in the radiative transport subroutine is to determine from the η coordinate values and the density distribution the physical thickness of the shock layer. The radiative flux divergence is then calculated at selected points and interpolated to yield values at all points across the shock layer. These flux divergence values are used along with the current velocity profile and Prandtl number variation to provide a new estimate for the enthalpy profile.

A test for convergence of the enthalpy profile is made at this point in the computational cycle. Further comments on the level of convergence to be expected will be given in Section 5. If satisfactory convergence has not been achieved, the entire iterative procedure is reinitiated. A number of investigators besides the author have observed the instability which arises if the calculated enthalpy profile is used unaltered as the enthalpy profile for the subsequent iterative cycle. In the absense of a meaningful stability analysis (which is likely to be impossible to achieve in view of the strong nonlinearity of the radiative transport terms), the following expedient has been employed. Let g^i be the current guess on the enthalpy profile and g^{i+1} the resulting calculated value. Then the next guess on the enthalpy profile which will be used to reinitiate the iterative loop is

$$g_{next} = (1-m)g^i + mg^{i+1}$$

where m is a fraction less than 1.0. A practical upper limit on m appears to be 0.5. As $m \to 0$ stability will undoubtedly be achieved but at the cost of numerous iterations for significant progress toward convergence. Our experience has shown that $m \sim 0.2$ to 0.3 are reasonable values for blowing problems while m may approach 0.5 for nonblowing.

If convergence is achieved or, as is more likely, a maximum number of iterative cycles have passed, then a final pass through the radiative transport subroutine is made. In this final pass the radiative flux at the wall is calculated using the unaltered enthalpy profile, $g = g^{i+1}$. This final wall

radiative flux value then can be compared against the value obtained from the enthalpy profile which existed upon the last entry to the energy equation. The comparison of these two flux values provides the best measure of convergence. Preparation of data for output, which is discussed in Section 4, completes the computation.

4. INPUT AND OUTPUT

4.1 Input Data

Table 1 lists the input data required to initiate a VISC code run. Also given in Table 1 is the data format, FORTRAN symbol and a synoptic description of each input quantity. The data is segregated into card groups. Depending on the amount of data required, more than one punched card may be needed in a given group. Figures 2 and 3 are copies from a computer listing of a set of input data. In the following discussion we shall proceed sequentially through Table 1. The reader will find it instructive to examine the typical values shown in Figs. 2 and 3 as we move through Table 1. The centimeter-gram-second system of units, along with °K for temperature, has been used for those input quantities given in dimensional form.

The data specified in the first card group is self-explanatory. The data specified in the second card group deals primarily with description of the free stream properties. Vehicle velocity and ambient density are self-explanatory. The quantity "vehicle size" is ambiguously described. This quantity is not necessarily the vehicle nose radius of curvature. This readily can be appreciated if we consider the case of a flat nose cylinder as our vehicle of interest for which the nose radius of curvature is infinite. The resolution of this ambiguity stems from the realization that in deriving the solution to the momentum equation the tangential velocity gradient is taken as unity at the shockwave.[8] Also, the Maslen approximation employed assumes a streamline curvature that is approximately that given by the shockwave curvature.[9] The above assumptions require that the normalizing dimension be the radius of curvature of an equivalent spherical body which supports a shockwave of known curvature. For spherical bodies it is reasonable to assume a concentric shockwave and the vehicle size is indeed in spherical nose radius. For extremely bluff bodies (e.g., an Apollo vehicle shape) some a priori information

Table 1

VISC Code Input Requirement

CARD GROUP	FORMAT	ITEM	DESCRIPTION
1	6A6	RUNID	Alphanumeric run identification
2	8E10.4	UINF	Vehicle velocity (cm/sec)
		RINF	Ambient density (gm/cm^3)
		XLF	Vehicle size (cm)
		GTW	Wall enthalpy or wall temperature, see ICWT, card 5
		RVW	Blowing rate (nondimensional)
		CANV	Convergence on energy equation
		XFT	Weighting factor in energy equation iteration
		TLH	Low to high species temperature switch (°K)
3	5E10.4	ALPH	Elemental mass fraction of H at wall
		ALPHE	Elemental mass fraction of He at wall
		ALPC	Elemental mass fraction of C at wall
		ALPN	Elemental mass fraction of N at wall
		ALPO	Elemental mass fraction of O at wall
4	5E10.4	CISH	Elemental mass fraction of H at shock
		CISHE	Elemental mass fraction of He at shock
		CISC	Elemental mass fraction of C at shock
		CISN	Elemental mass fraction of N at shock
		CISO	Elemental mass fraction of O at shock
5	8I5	NES	Number of shock layer points (max 35)
		IEZ	Number of shock layer points at which $\nabla \cdot q$ is calc. (max 25)
		ITGS	Maximum number of iterations
		IO	= 0 no radiation; = 1 with radiation
		MOL	= 0 without molecules; = 1 with molecules
		LINES	= 0 without lines; = 1 with lines
		ICWT	= 0 wall enthalpy input; = 1 wall temperature
		IDG	= 0 no diagnostic O/P; = 1 diagnostic O/P

Table 1 (Continued)

CARD GROUP	FORMAT	ITEM	DESCRIPTION
6	8E10.4	ETA(I),I=1,NES	η-coordinate mesh points
7	8E10.4	F(I),K=1,NES	Velocity profile guess
8	8E10.4	CV(I),I=1,NES	Blown gas mass fraction profile (if RVW = 0, input CV(I) = 0)
9	8E10.4	G(I),I=1,NES	Enthalpy profile guess
10	1615	IETZ(J),J=1,IEZ	Subscript I of ETA(I) at which $\nabla \cdot q$ is calculated

```
VISC - VISCOUS RADIATING STAGNATION POINT FLOW CODE                CASE 3 - BLOWING

VEHICLE AND FLIGHT CONDITIONS

 VEHICLE VELOCITY =   4.0000+06 CM/SEC
  AMBIENT DENSITY =   6.9000-07 GM/CM3
     VEHICLE SIZE =   1.5900+01 CM
 AMBIENT ENTHALPY =   0.0000     ERGS/GM
 WALL TEMPERATURE =   4.5000+03 DEG.K
     BLOWING RATE =   4.0000-01 NORMALIZED


COMPOSITION BY ELEMENTAL MASS FRACTION

              ATMOSPHERE     HEAT SHIELD
   HYDROGEN       .740          .000
     HELIUM       .260          .000
     CARBON       .000         1.000
   NITROGEN       .000          .000
     OXYGEN       .000          .000


PROGRAM OPTIONS AND PARAMETERS

    5.0  PRECENT CONVERGENCE ON ENERGY EQUATIONS
    .20  WEIGHTING FACTOR IN ENTHALPY PROFILE SPECIFICATION
  7000.  LOW TO HIGH TEMPERATURE SPECIES SWITCH (DEG.K)
     27  SHOCK LAYER POINTS
     22  SHOCK LAYER POINTS FOR FLUX DIVERGENCE
      1  MAXIMUM ITERATIONS

         COUPLED RADIATIVE TRANSPORT
         MOLECULAR ABSORPTION INCLUDED IN RADIATIVE TRANSPORT
         ATOMIC LINES INCLUDED IN RADIATIVE TRANSPORT
         WALL TEMPERATURE SPECIFIED
         DIAGNOSTIC DATA REQUESTED
```

Fig. 2 - Input Data: Vehicle and Atmospheric Parameters

INITIAL SHOCK LAYER PROFILES

ETA	F	CV	G	Q-POINT
0.00000	0.00000	1.00000+00	-2.80000-03	*
2.00000-01	9.10000-03	1.00000+00	-1.20000-03	*
4.00000-01	1.90000-02	1.00000+00	1.20000-03	*
5.00000-01	2.40000-02	1.00000+00	3.30000-03	*
6.00000-01	3.00000-02	1.00000+00	7.10000-03	*
7.00000-01	3.80000-02	1.00000+00	1.40000-02	*
7.50000-01	4.30000-02	9.90000-01	1.90000-02	*
8.00000-01	5.00000-02	9.80000-01	2.80000-02	*
8.20000-01	5.40000-02	9.70000-01	3.20000-02	*
8.40000-01	5.90000-02	9.60000-01	3.90000-02	*
8.60000-01	6.70000-02	9.50000-01	5.00000-02	*
8.70000-01	7.30000-02	9.30000-01	5.80000-02	
8.80000-01	8.10000-02	9.00000-01	7.60000-02	*
8.90000-01	9.60000-02	8.60000-01	1.00000-01	*
9.00000-01	1.30000-01	7.80000-01	1.50000-01	*
9.05000-01	1.70000-01	7.00000-01	2.00000-01	
9.10000-01	2.90000-01	4.50000-01	4.20000-01	*
9.20000-01	5.30000-01	0.00000	8.30000-01	*
9.30000-01	5.90000-01	0.00000	8.80000-01	*
9.40000-01	6.50000-01	0.00000	9.10000-01	*
9.50000-01	7.10000-01	0.00000	9.30000-01	
9.60000-01	7.70000-01	0.00000	9.50000-01	*
9.70000-01	8.30000-01	0.00000	9.60000-01	
9.80000-01	8.90000-01	0.00000	9.70000-01	*
9.90000-01	9.40000-01	0.00000	9.80000-01	*
9.95000-01	9.70000-01	0.00000	9.90000-01	*
1.00000+00	1.00000+00	0.00000	1.00000+00	

Fig. 3 - Input Data: Initial Shock Layer Profiles

on shockwave curvature must be known in order to obtain the effective spherical nose which will support that shockwave. Only in this manner will the correct shock layer thickness be obtained.

The requirement for specifying free stream enthalpy is a result of recent interest in applying the VISC code to Venus entry problems. Normally the vehicle velocity is so large that $h_\infty/U_\infty^2/2 \ll 1$ and the free stream enthalpy is quite negligible. However, care must be exercised in those cases where the ambient gas is composed of significant amounts of polyatomic species such as CO_2 or H_2O. The FEMP routine uses an accounting system which sets the energy of formation of diatomic species (N_2, C_2, O_2, H_2) equal to zero. The triatomic species H_2O and CO_2 have a large negative enthalpy in this system. Only by specifying that negative enthalpy in the input data is the calculation able to correctly soak up the amount of energy expended in dissociating these triatomic molecules. Neglecting the intrinsic enthalpy, the free stream enthalpy for a gas containing only diatomics and H_2O and CO_2 is

$$h_\infty = \alpha_{H_2O} E^\circ_{H_2O} + \alpha_{CO_2} E^\circ_{CO_2}$$

where the energies of formation are $E^\circ_{H_2O} = 1.71 \times 10^{11}$ erg/gm and $E^\circ_{CO_2} = 1.33 \times 10^{11}$ erg/gm. In this expression α_{H_2O} and α_{CO_2} are the mass fractions of H_2O and CO_2.

The wall is characterized by either a prescribed enthalpy or (normally) temperature according to an option given in card group 5. If a prescribed wall enthalpy is input, that enthalpy must be normalized to the total free stream enthalpy $h_\infty + U_\infty^2/2$. If a prescribed wall temperature is used, the value is input in dimensional (°K) form.

The blowing rate is given in terms of a normalized value $m \equiv \rho_w V_w/\rho_\infty U_\infty$. It should be emphasized that the blowing rate is held constant during any given run. The blowing rate specification is further discussed in Section 5.

The convergence criterion τ is applied by requiring

$$\frac{g^{i+1} - g^{i}}{(g^{i+1} + g^{i})/2} < \tau$$

be satisfied at all shock layer points in order for convergence to be achieved. For nonblowing problems, convergence to a level of $\tau = .01$ (i.e., 1% convergence) is an achievable goal. However, for radiative dominated problems, a 1% convergence tolerance is probably too severe. Usually a few points in the shock layer hold-up convergence. Hence, when a 1% convergence level is achieved the radiative flux at the wall is changing considerably less than 1% between iterations. A precision of 1% is inconsistent with the overall accuracy of the optical properties, transport properties and the assumption of chemical equilibrium which set the true error bound on the heating predictions. For blowing problems, convergence to a 5% level is rarely achieved. For blowing problems, convergence is much more reasonably measured by comparing the wall flux based on the final guessed and calculated enthalpy profile.

The weighting factor employed in stabilizing the successive iterations on the energy equation was discussed in the previous section.

The FEMP routine considers two different temperature ranges. These two ranges are denoted as the low temperature regime and the high temperature regime. The low temperature regime does not contain ionized species whereas the high temperature regime does not contain polyatomic species. A tabulation of the species considered in each temperature regime is given in Table I of Ref. 7. Changes to that tabulation since it was published include: (1) addition of C_3, He, H_2O and CO_2 to the low temperature regime; (2) addition of C_2, He and He^+ to the high temperature regime. The VISC code user must specify a temperature at which the FEMP calculation is switched from the low to high regimes. Selection of this low to high temperature break-point must take into consideration that it should be sufficiently high that polyatomic species would not be present in significant amounts ($\lesssim$ 1%) at or above that temperature nor ionized species present in significant amounts at or below that temperature. The temperature break-point will depend on the stagnation-point pressure and typically will vary from 5000°K at low pressures ($\sim$ 0.1 atm) to 8000°K at high pressures ($\sim$ 100 atm). The solution is not critically dependent on the value

of the break-point temperature selected. With a little experience in a given problem, an appropriate value for the temperature switch will be readily apparent to the user. An additional requirement is that the low to high temperature switch be greater than the wall temperature but less than the shock temperature.

The third and fourth card groups permit specification of an arbitrary ablation product (card group 3) and atmospheric (card group 4) gas composition. A fundamental restriction on the VISC code is that the composition of ablator and atmosphere be comprised of H, He, C, N and O elements. The species included in the FEMP routine were selected on the basis of being the most significant for a mixture comprised of these elements.[4,7] For both ablator or atmosphere the composition is given simply on an elemental mass fraction basis. The actual species composition of the gases entering the shock layer is not specified as this will be handled by FEMP.

The fifth card group provides control options. The number of shock layer points is at the discretion of the user. Storage limitations require that the number of shock layer points be kept equal to or less than 35. As was mentioned above, the radiative flux divergence is not necessarily calculated at every shock layer point. Storage limitations require that the number of shock layer points at which the flux divergence is calculated be equal to or less than 25. When the number of shock layer points exceeds the number of flux divergence points, an interpolation procedure is used to determine the flux divergence at the noncalculated points.

The maximum number of iterations provides a termination point for the calculation when "convergence" of the enthalpy profile is not achieved. On the UNIVAC 1108 EXEC 8 system in operation at LMSC, the computation time for a full iterative cycle (i.e., solution of momentum, mass and energy equations including FEMP and TRANS subroutines) for a typical problem involving 30 shock layer points and 25 flux divergence points is approximately 1 minute. Computer time, then, is normally the overriding consideration in selection of the maximum number of iterations.

The remaining quantities in card group 5 are self-explanatory options. With regard to the diagnostic output, there will not be a discussion of the diagnostic data in Section 4.2. Without extensive study of the code details, the diagnostic data would have no utility to the user.

The last sequence of card groups specifies the computational grid (in the η-coordinate) and initial estimates of the normalized tangential velocity F , blown gas mass fraction CV, and normalized enthalpy G profiles. Also specified are the η-points at which the flux divergence is evaluated, denoted by Q-POINT in Fig. 3. These estimates, of course, are crucial and a discussion of input profiles will be given in Section 5.

In addition to the normal input listed in Table 1, the user may also specify the spectral emissivity of the wall to account for surface emission and reflection. It was felt that it would be an inconvenience to require this spectral emissivity data to be input for every run. In a typical application of the VISC code, we expect the surface properties to be fixed for a number of cases in which the atmospheric and vehicle parameters are varied. Accordingly, the spectral emissivity data are specified in an internally programmed data statement at the beginning of TRANS, the radiative transport subroutine. The data is specified in terms of the average emissivity within each of the 26 spectral groups employed in the continuum transport evaluation. That is to say, the VISC code currently represents the spectral variation of surface emissivity by average values at 26 locations across the spectrum. The frequency values of the continuum groups are evident from the output discussed in the next subsection. For the line transport, the VISC code lifts the surface emissivity values appropriate to the frequency interval of the various line groups in exactly the same way it determines the appropriate underlying continuum optical depth for each line group. Currently, the VISC code is programmed with unit surface emissivity for each continuum spectral interval.

4.2 Output Data

Figures 4 through 13 display copies of the computer listing of the output data for the problem defined by the set of input data shown in Figs. 2

and 3. In Fig. 4, the thermodynamic properties behind the normal shock are shown. In addition, the density jump ρ_∞/ρ_s and the Reynolds number $Re_s \equiv \rho_s U_\infty R/\mu s$ are output. Also included on Fig. 4 is a status report on the last energy equation iteration in terms of a comparison between the guessed and calculated enthalpy profile.

Figure 5 summarizes the radiative flux picture. Both the continuum and line fluxes (in W/cm^2) at the wall Q + (0) and shock Q - (1) are given as a function of the continuum and line group and, for convenience, the average spectral values (in W/cm^2 eV) in each group were output. The final quantity in Fig. 5 is the integral of the radiative flux divergence over the shock layer. This integral is to be compared with the sum of the continuum and line total fluxes (i.e., spectral summation) emergent from shock layer at the wall and shock. Agreement of the flux divergence integral with the total summation of all flux components demonstrates adequate spatial resolution of the flux divergence calculation across the shock layer.

The radiative flux is calculated at the same time the flux divergence is calculated. This allows us to present the radiative flux distribution across the shock layer in terms of the flux values at each of the Q-POINT locations. Figure 6 shows a representative set of this radiative flux data. The η coordinate and corresponding physical coordinate (normalized to total shock layer thickness) are indicated. This is followed by a listing of the continuum and line fluxes, in W/cm^2, and the spectral summation. The spectral continuum optical depth evaluated at the midpoint of each continuum or line group is presented along with the flux values.

At the termination of the radiative flux output at the last shock layer point, $\eta = 1$, the wall convective and radiative heating values are presented. This is shown in Fig. 7. Of course, the radiative flux value was already output in terms of the continuum and line components in Fig. 5. These two radiative flux components are simply summed and repeated for convenience in the output indicated by Fig. 7. In addition to the absolute heating values, a convective and radiative heat transfer coefficient, defined as the heating rates normalized by $1/2\ \rho_\infty U_\infty^3$, is presented as shown in Fig. 7

CONDITIONS BEHIND NORMAL SHOCK

PRESSURE = 9.8440+00 ATMS

SHOCK LAYER THICKNESS = 1.1691+00 CM

ENTHALPY = 0.0014+12 ERGS/GM
TEMPERATURE = 1.6554+04 DEG.K
DENSITY = 7.1800-06 GM/CM3
DENSITY JUMP = 9.6460-02
VISCOSITY = 5.9562-04 GM/CM-SEC
REYNOLDS NUMBER = 7.6656+05

LAST ENTHALPY PROFILE ITERATION

ETA	F	CV	G(GUESS)	G(CALC)
0.00000	0.00000	1.00000+00	-2.82754-03	-2.82754-03
2.00000-01	8.96814-03	9.99999-01	-1.20394-03	-1.35208-03
4.00000-01	1.86843-02	9.99992-01	1.19622-03	1.07914-03
5.00000-01	2.40215-02	9.99978-01	3.29001-03	3.16435-03
6.00000-01	3.01311-02	9.99934-01	7.07877-03	6.60569-03
7.00000-01	3.78450-02	9.99771-01	1.39710-02	1.27092-02
7.50000-01	4.32161-02	9.99516-01	1.83370-02	1.75257-02
8.00000-01	5.10510-02	9.98739-01	2.39569-02	2.44792-02
8.20000-01	5.54637-02	9.97978-01	2.49242-02	2.83371-02
8.40000-01	6.12224-02	9.96512-01	2.81765-02	3.34427-02
8.60000-01	7.00904-02	9.93266-01	3.63982-02	4.22553-02
8.70000-01	7.59429-02	9.89928-01	3.88179-02	5.01527-02
8.80000-01	8.76592-02	9.82916-01	5.07054-02	6.20446-02
8.90000-01	1.05781-01	9.64630-01	6.47155-02	7.96669-02
9.00000-01	1.42158-01	9.04324-01	1.01621-01	1.12429-01
9.05000-01	1.84318-01	8.11344-01	1.52821-01	1.54127-01
9.10000-01	3.14375-01	4.97856-01	3.94614-01	3.92426-01
9.20000-01	5.27444-01	2.15824-05	8.26418-01	8.40072-01
9.30000-01	5.93674-01	0.00000	8.78410-01	9.06128-01
9.40000-01	6.54000-01	0.00000	9.04860-01	9.30359-01
9.50000-01	7.13112-01	0.00000	9.26192-01	9.46621-01
9.60000-01	7.71192-01	0.00000	9.46656-01	9.59216-01
9.70000-01	8.28762-01	0.00000	9.58227-01	9.69564-01
9.80000-01	8.86583-01	0.00000	9.68507-01	9.79382-01
9.90000-01	9.43174-01	0.00000	9.78609-01	9.86688-01
9.95000-01	9.71624-01	0.00000	9.88688-01	9.92173-01
1.00000+00	1.00000+00	0.00000	9.98764-01	1.00000+00

Fig. 4 - Output Data: Normal Shock Conditions and Status of Enthalpy Iteration

WALL AND SHOCK RADIATIVE FLUXES - SPECTRAL DISTRIBUTION

CONTINUUM CONTRIBUTION TO THE SPECTRAL FLUX

K	HNU	DHNU	Q+(0)	Q+/DHNU	Q-(1)	Q-/DHNU
1	,480	.500	6,691+02	1,338+03	7.355+02	1,471+03
2	1,140	.660	3,126+03	4,737+03	3.848+03	5,830+03
3	1,600	.460	2,936+03	6,383+03	3.562+03	7,743+03
4	2,000	.400	1,980+03	4,949+03	2.423+03	6,056+03
5	2,900	.900	6,995+02	7,773+02	4.045+03	4,495+03
6	3,200	.300	8,716+01	2,905+02	8.729+02	2,910+03
7	3,500	.300	2,959+03	9,863+03	3.569+03	1,190+04
8	4,000	.500	3,353+03	6,705+03	4.631+03	9,261+03
9	4,500	.500	2,095+03	4,191+03	3.316+03	6,633+03
10	5,000	.500	1,208+03	2,416+03	2.354+03	4,708+03
11	5,500	.500	1,228+03	2,456+03	1.657+03	3,314+03
12	6,000	.500	1,108+03	2,216+03	1.164+03	2,329+03
13	6,500	.500	7,864+02	1,573+03	8.175+02	1,635+03
14	7,000	.500	5,718+02	1,144+03	5.730+02	1,146+03
15	7,500	.500	3,542+02	7,083+02	4.014+02	8,027+02
16	8,000	.500	1,145+01	2,290+01	2.824+02	5,648+02
17	8,370	.370	1,255+00	3,393+00	1.534+02	4,145+02
18	9,000	.630	1,904+00	3,022+00	2.404+02	3,816+02
19	9,500	.500	9,317+01	1,863+02	1.308+02	2,617+02
20	9,790	.290	5,665+01	1,953+02	5.845+01	2,015+02
21	10,770	.980	2,050+02	2,092+02	6.408+02	6,539+02
22	11,050	.280	4,055+01	1,448+02	1.276+02	4,556+02
23	11,950	.900	1,014-04	1,127-04	9.446+02	1,050+03
24	13,400	1.450	7,204-05	4,968-05	8.033+02	5,540+02
25	14,330	.930	1,938-05	2,084-05	2.331+03	2,506+03
26	20,000	5.670	2,393-05	4,221-06	3.659+03	6,453+02
TOTAL FLUX			2.357+04		4,334+04	

LINE CONTRIBUTION TO THE SPECTRAL FLUX

J	HNUC	DHNU	Q+(0)	Q+/DHNU	Q-(1)	Q-/DHNU
1	1,300	.600	1,477+02	2,462+02	1.765+02	2,942+02
2	1,900	.600	4,669+03	7,781+03	5.262+03	8,770+03
3	2,700	.600	4,022+02	6,703+02	7.937+03	1,323+04
4	7,250	.500	1,712+02	3,425+02	6.035+02	1,207+03
5	8,050	.700	7,564+00	1,081+01	2.618+03	3,740+03
6	9,100	1.400	8,456+02	6,040+02	5.343+03	3,816+03
7	10,300	1.000	3,428+02	3,428+02	8.238+03	8,238+03
8	10,950	.300	-4,128+01	-1,376+02	4.864+02	1,621+03
9	11,550	.900	0,000	0,000	0.000	0,000
10	12,700	1.400	4,730-05	3,379-05	4.678+03	3,341+03
11	13,900	1.000	-1,467-07	-1,467-07	3.002-13	3,002-13
TOTAL FLUX			6.545+03		3,534+04	

TOTAL FLUX DIVERGENCE INTEGRATION = 1,0217+05

Fig. 5 - Output Data: Radiative Flux at Wall and Shock

SHOCK LAYER RADIATIVE TRANSPORT SUMMARY

CONTINUUM CONTRIBUTION

		(ETA= ,000 Y/D= 0,000)			(ETA= ,200 Y/D= 1,874-02)			(ETA= ,400 Y/D= 3,901-02)		
GP	HNU1-HNU2	POS.FLUX	NEG.FLUX	OPT.DEP.	POS.FLUX	NEG.FLUX	OPT.DEP.	POS.FLUX	NEG.FLUX	OPT.DEP.
1	,0- ,5	6,691+02	1,386+02	0,000	6,691+02	1,386+02	2,533-09	6,691+02	1,386+02	1,035-08
2	,5- 1,1	3,128+03	7,332+02	0,000	3,175+03	7,337+02	2,045-02	3,234+03	7,354+02	4,467-02
3	1,1- 1,6	2,936+03	5,601+02	0,000	2,970+03	5,605+02	1,425-02	3,009+03	5,619+02	3,102-02
4	1,6- 2,0	1,980+03	3,631+02	0,000	1,997+03	3,633+02	1,085-02	2,018+03	3,643+02	2,432-02
5	2,0- 2,9	6,995+02	3,092+02	0,000	8,673+02	4,115+02	4,856-01	1,149+03	4,536+02	1,064+00
6	2,9- 3,2	8,716+01	5,255+01	0,000	1,141+02	5,521+01	6,561-01	1,644+02	6,407+01	1,436+00
7	3,2- 3,5	2,959+03	3,213+01	0,000	3,024+03	3,221+01	2,216-02	3,110+03	3,257+01	5,042-02
8	3,5- 4,0	3,353+03	2,732+01	0,000	3,488+03	2,746+01	3,989-02	3,668+03	2,807+01	9,076-02
9	4,0- 4,5	2,095+03	1,099+01	0,000	2,233+03	1,109+01	6,415-02	2,417+03	1,154+01	1,438-01
10	4,5- 5,0	1,208+03	4,237+00	0,000	1,339+03	4,308+00	1,036-01	1,517+03	4,610+00	2,288-01
11	5,0- 5,5	1,228+03	1,579+00	0,000	1,292+03	1,594+00	5,051-02	1,371+03	1,658+00	1,099-01
12	5,5- 6,0	1,108+03	5,726-01	0,000	1,115+03	5,734-01	6,561-03	1,124+03	5,771-01	1,470-02
13	6,0- 6,5	7,864+02	2,029-01	0,000	7,905+02	2,031-01	5,103-03	7,955+02	2,043-01	1,144-02
14	6,5- 7,0	5,718+02	7,049-02	0,000	5,718+02	7,049-02	5,811-06	5,718+02	7,049-02	1,343-05
15	7,0- 7,5	3,542+02	2,409-02	0,000	3,610+02	2,422-02	1,919-02	3,695+02	2,484-02	4,236-02
16	7,5- 8,0	1,145+01	8,114-03	0,000	1,885+01	9,103-03	4,989-01	3,442+01	1,321-02	1,101+00
17	8,0- 8,4	1,255+00	2,254-03	0,000	2,650+00	2,651-03	7,483-01	6,535+00	4,231-03	1,652+00
18	8,4- 9,0	1,904+00	1,332-03	0,000	4,023+00	1,583-03	7,486-01	9,930+00	2,603-03	1,653+00
19	9,0- 9,5	9,317+01	2,890-04	0,000	9,776+01	2,943-04	4,818-02	1,036+02	3,209-04	1,065-01
20	9,5- 9,8	5,665+01	6,631-05	0,000	5,666+01	6,631-05	2,112-04	5,668+01	6,635-05	5,738-04
21	9,8-10,8	2,050+02	6,328-05	0,000	2,113+02	6,412-05	3,035-02	2,216+02	6,970-05	7,758-02
22	10,8-11,1	4,055+01	3,846-06	0,000	4,180+01	3,898-06	3,035-02	4,382+01	3,959-06	7,758-02
23	11,1-12,0	1,014-04	3,411-06	0,000	2,408-04	4,457-06	8,954-01	8,356-04	9,533-06	2,175+00
24	12,0-13,4	7,204-05	4,631-07	0,000	1,753-04	6,228-07	8,954-01	6,254-04	1,433-06	2,175+00
25	13,4-14,3	1,938-05	1,412-08	0,000	4,742-05	1,981-08	8,954-01	1,703-04	5,055-08	2,175+00
26	14,3-20,0	2,393-05	1,754-09	0,000	5,859-05	2,543-09	8,954-01	2,105-04	7,034-09	2,175+00
		2,357+04	2,324+03		2,444+04	2,340+03		2,566+04	2,397+03	

LINE CONTINBUTION

		(ETA= ,000 Y/D= 0,000)			(ETA= ,200 Y/D= 1,874-02)			(ETA= ,400 Y/D= 3,901-02)		
GP	HNU1-HNU2	POS.FLUX	NEG.FLUX	OPT.DEP.	POS.FLUX	NEG.FLUX	OPT.DEP.	POS.FLUX	NEG.FLUX	OPT.DEP.
1	1,0- 1,6	1,477+02	0,000	0,000	1,499+02	0,000	1,425-02	1,524+02	2,079-05	3,102-02
2	1,6- 2,2	4,669+03	0,000	0,000	4,720+03	0,000	1,085-02	4,784+03	1,747-07	2,432-02
3	2,4- 3,0	4,022+02	0,000	0,000	6,536+02	0,000	4,856-01	1,166+03	0,000	1,064+00
4	7,0- 7,5	1,712+02	0,000	0,000	1,755+02	0,000	1,919-02	1,809+02	1,483-04	4,236-02
5	7,7- 8,4	7,564+00	0,000	0,000	1,601+01	0,000	7,483-01	3,960+01	2,938-05	1,652+00
6	8,4- 9,8	8,456+02	0,000	0,000	8,876+02	0,000	4,818-02	9,412+02	1,341-05	1,065-01
7	9,8-10,8	3,428+02	0,000	0,000	3,534+02	0,000	3,035-02	3,705+02	3,037-07	7,758-02
8	10,8-11,1	-4,128+01	0,000	0,000	-4,249+01	0,000	3,035-02	-4,444+01	6,905-08	7,758-02
9	11,1-12,0	0,000	0,000	0,000	0,000	0,000	8,954-01	0,000	0,000	2,175+00
10	12,0-13,4	4,730-05	0,000	0,000	1,159-04	0,000	8,954-01	4,166-04	7,627-10	2,175+00
11	13,4-14,4	-1,467-07	0,000	0,000	-3,582-07	0,000	8,954-01	-1,283-06	5,361-12	2,175+00
		6,545+03	0,000		6,913+03	0,000		7,590+03	2,124-04	

Fig. 6 - Output Data: Typical Radiative Flux Data at Selected Shock Layer Points

LINE CONTINBUTION

		(ETA= .998 Y/D= 9.488-01)			(ETA= 1.000 Y/D= 1.000+00)		
GP	HNU1-HNU2	POS.FLUX	NEG.FLUX	OPT.DEP.	POS.FLUX	NEG.FLUX	OPT.DEP.
1	1.0- 1.6	4.891-02	1.805+02	3.918-01	0.000	1.765+02	4.143-01
2	1.6- 2.2	1.339+03	5.120+03	2.289-01	0.000	5.262+03	2.400-01
3	2.4- 3.0	7.108+02	7.524+03	3.052+00	0.000	7.037+03	3.057+00
4	7.0- 7.5	0.000	6.046+02	1.464-01	0.000	6.033+02	1.480-01
5	7.7- 8.4	0.000	2.621+03	4.826+00	0.000	2.618+03	4.827+00
6	8.4- 9.8	0.000	5.347+03	3.558-01	0.000	5.343+03	3.566-01
7	9.8-10.8	3.852+03	7.997+03	1.280+00	0.000	8.238+03	1.290+00
8	10.8-11.1	0.000	4.864+02	1.288+00	0.000	4.864+02	1.288+00
9	11.1-12.0	0.000	0.000	1.692+01	0.000	0.000	1.692+01
10	12.0-13.4	3.871+03	4.511+03	1.692+01	0.000	4.673+03	1.692+01
11	13.4-14.4	0.000	1.517-12	4.688+01	0.000	3.002-13	4.850+01
		9.772+03	3.439+04		0.000	3.634+04	

HEAT TRANSFER VALUES

CONVECTIVE FLUX = 1.2642+02 W/CM2

CONVECTIVE FLUX COEFFICIENT = 2.8628-05

SURFACE RADIATIVE FLUX = 3.0116+04 W/CM2

SURFACE RADIATIVE FLUX COEFFICIENT = 6.8197-03

Fig. 7 - Output Data: Convective and Radiative Fluxes

A summary of the final values of the gasdynamic quantities--stream function, tangential velocity, enthalpy, ablation product mass fraction, flux divergence (W/cm^3) and a repeat of the Q-POINT location--is output next. A representative set is shown as Fig. 8. A quick comparison between the initial and final profiles is thus available by examining the data of Figs. 3 and 8. It will be observed that the enthalpy tabulated in Fig. 8 is the weighted average of the final guessed and calculated values shown in Fig. 4. Thus this enthalpy profile represents the input to the next iteration. In principal, the output shown in Fig. 8 can be used directly to initiate a new set of iterations.

A summary of the thermodynamic and collisional transport properties consistent with the gasdynamic data given in Fig. 8 is the next data output. A representative set is shown as Fig. 9.

The next series of output presents the molecular and atomic species number density distributions across the shock layer. A representative set for the molecular species is shown as Fig. 10 and likewise for the atomic species as Fig. 11.

The final computation which the VISC code performs is an evaluation of the radiative flux at the wall using the unaltered calculated enthalpy profile (as opposed to the profile weighted between guessed and calculated values) from the last iteration. The representative values of output which describes this final calculation is shown as Fig. 12. In Fig. 12, data from the FEMP routine is displayed with the temperature variable being of maximum interest. The final output gives the continuum and line flux which may be compared with the data shown on Fig. 5 to assess the level of convergence of the overall radiative flux determination.

SHOCK LAYER GASDYNAMIC SUMMARY

ETA	Y/D	PSI	F	G	GV	Q	Q-POINT
0.00000	0.00000	-1.68908+01	0.00000	-2.82754+03	1.00000+00	-4.77840+04	*
2.00000-01	1.87399-02	-1.63118+01	8.96814-03	-1.28336+03	9.99999-01	-6.58498+04	*
4.00000-01	3.90117-02	-1.45265+01	1.86843-02	1.17640+03	9.99992-01	-9.33507+04	*
5.00000-01	5.00562-02	-1.31489+01	2.40215-02	3.26478+03	9.99978-01	-1.22246+05	*
6.00000-01	6.21515-02	-1.14037+01	3.01011-02	6.94415+03	9.99934-01	-1.61930+05	*
7.00000-01	7.44914-02	-9.21256+00	3.78455-02	1.37186+02	9.99771-01	-1.98192+05	*
7.50000-01	8.48944-02	-7.90561+00	4.32161-02	1.81747+02	9.99516-01	-2.15232+05	*
8.00000-01	9.44889-02	-6.38625+00	5.10511-02	2.40614+02	9.98739-01	-2.11597+05	*
8.20000-01	9.86737-02	-5.69992+00	5.54037-02	2.56068+02	9.97978-01	-2.14245+05	*
8.40000-01	1.03109-01	-4.94780+00	6.12226-02	2.92276+02	9.96512-01	-1.90698+05	*
8.60000-01	1.08273-01	-4.10026+00	7.00904-02	3.75676+02	9.93266-01	-1.37157+05	*
8.70000-01	1.11220-01	-3.62517+00	7.69429-02	4.11846+02	9.89928-01	-1.44205+05	
8.80000-01	1.14455-01	-3.09264+00	8.76592-02	5.24733+02	9.82916-01	-1.55252+05	*
8.90000-01	1.20928-01	-2.46494+00	1.03781-01	6.77068+02	9.64630-01	-2.73456+05	*
9.00000-01	1.28437-01	-1.65194+00	1.42158-01	1.01703+01	9.04324-01	-2.72803+05	*
9.05000-01	1.35343-01	-1.10856+00	1.84318-01	1.53002+01	8.11344-01	-6.14759+04	
9.10000-01	1.50557-01	-2.70753-01	3.14375-01	3.94177+01	4.97856-01	1.09651+05	*
9.20000-01	2.17299-01	2.50365+00	5.27444-01	8.24149+01	2.15824-05	1.68328+05	*
9.30000-01	3.08457-01	6.14055+00	5.93074-01	8.81953+01	0.00000	9.56379+04	*
9.40000-01	4.03434-01	1.01734+01	6.54000-01	9.03900+01	0.00000	9.29625+04	*
9.50000-01	4.99842-01	1.45864+01	7.13119-01	9.30278+01	0.00000	9.75283+04	
9.60000-01	5.97850-01	1.93740+01	7.71193-01	9.49168+01	0.00000	1.02694+05	*
9.70000-01	6.97382-01	2.45333+01	8.28762-01	9.64494+01	0.00000	1.07491+05	
9.80000-01	7.97150-01	3.00637+01	8.86083-01	9.74402+01	0.00000	1.12889+05	*
9.90000-01	8.97996-01	3.59621+01	9.43174-01	9.83225+01	0.00000	1.36825+05	*
9.95000-01	9.48805-01	3.90486+01	9.71624-01	9.87345+01	0.00000	2.36076+05	*
1.00000+00	1.00000+00	4.22270+01	1.00000+00	9.99012+01	0.00000	5.35329+05	

Fig. 8 - Output Data: Shock Layer Gasdynamic Variables

SHOCK LAYER THERMODYNAMIC AND TRANSPORT SUMMARY

ETA	Y/D	H (ERGS/GM)	R (GM/CM3)	MU (GM/CM-SEC)	RM, (GM2/CM4-SEC)	T (DEG.K)	PR	CPR (ERGS/GM-DEG.K)	KR (ERGG/CM-SEC-DEG.K)
.0000	0.0000	-2.2624+10	8.1444-04	1.2358-03	1.0064-06	4.5000+03	4.4570-01	1.0699+08	2.9658+05
.2000	1.6740-02	-9.6331+09	7.6236-04	1.2661-03	9.6523-07	4.6121+03	4.5533-01	1.2616+08	3.5095+05
.4000	3.9012-02	9.5714+09	6.9666-04	1.3049-03	9.0908-07	4.7510+03	4.7464-01	1.5233+08	4.1872+05
.5000	5.0036-02	2.6325+10	6.6749-04	1.3249-03	8.8436-07	4.8248+03	4.9463-01	1.7277+08	4.6621+05
.6000	6.2151-02	5.4640+10	6.7231-04	1.3650-03	7.9262-07	5.0480+03	5.3026-01	1.9685+08	5.1404+05
.7000	7.6491-02	1.1179+11	4.6745-04	1.4686-03	6.8651-07	5.3109+03	6.1439-01	2.2251+08	5.3196+05
.7500	8.4854-02	1.4672+11	4.1409-04	1.5215-03	6.3125-07	5.4685+03	6.7345-01	2.2319+08	5.0416+05
.8000	9.4489-02	1.9169+11	3.5767-04	1.5922-03	5.6949-07	5.6743+03	7.5536-01	2.0870+08	4.3983+05
.8200	9.8674-02	2.0943+11	3.4780-04	1.6031-03	5.5755-07	5.7066+03	7.7114-01	2.0753+08	4.3133+05
.8400	1.0311-01	2.2545+11	3.1699-04	1.6428-03	5.2405-07	5.8246+03	8.2142-01	1.9333+08	3.8658+05
.8600	1.0827-01	2.4124+11	2.5686-04	1.7592-03	4.5538-07	6.1444+03	9.4440-01	1.3452+08	2.5053+05
.8700	1.1122-01	3.1060+11	2.4235-04	1.7814-03	4.3172-07	6.2700+03	9.7155-01	1.2249+08	2.2456+05
.8800	1.1455-01	4.0571+11	1.7469-04	1.9678-03	3.4724-07	7.3619+03	8.6045-01	4.2661+07	9.8534+04
.8900	1.2003-01	5.1781+11	1.2052-04	2.0710-03	2.4357-07	9.0801+03	7.1167-01	3.8373+07	1.0895+05
.9000	1.2644-01	6.1311+11	6.9008-05	1.6338-03	1.1273-07	1.0990+04	7.4720-01	7.7324+07	1.6904+05
.9050	1.3534-01	1.2220+12	4.3589-05	1.3564-03	5.9123-08	1.1899+04	8.0134-01	1.2700+08	2.1493+05
.9100	1.5036-01	3.1575+12	1.6796-05	8.9567-04	1.5046-08	1.4278+04	1.2472+00	4.0435+08	2.2033+05
.9200	2.1730-01	6.4125+12	8.2399-06	6.9442-04	5.7219-09	1.9456+04	1.9196+00	9.0343+08	3.2675+05
.9300	3.0896-01	7.0285+12	7.8869-06	6.6286-04	5.2121-09	1.9810+04	1.9579+00	9.6044+08	3.2411+05
.9400	4.0343-01	7.2401+12	7.7195-06	6.4513-04	4.9801-09	1.9982+04	1.9731+00	9.8705+08	3.2268+05
.9500	4.9984-01	7.4108+12	7.5696-06	6.3506-04	4.8048-09	1.9117+04	1.9834+00	1.0073+09	3.2146+05
.9600	5.9785-01	7.5745+12	7.4696-06	6.2196-04	4.6458-09	1.9243+04	1.9919+00	1.0256+09	3.2035+05
.9700	6.9736-01	7.6671+12	7.4033-06	6.1587-04	4.5595-09	1.9314+04	1.9961+00	1.0356+09	3.1954+05
.9800	7.9715-01	7.7494+12	7.3454-06	6.1059-04	4.4850-09	1.9376+04	1.9995+00	1.0445+09	3.1889+05
.9900	8.9690-01	7.8302+12	7.2893-06	6.0549-04	4.4136-09	1.9436+04	2.0026+00	1.0527+09	3.1824+05
.9950	9.4691-01	7.9109+12	7.2343-06	6.0051-04	4.3442-09	1.9495+04	2.0054+00	1.0608+09	3.1758+05
1.0000	1.0000+00	7.9915+12	7.1800-06	5.9562-04	4.2766-09	1.9554+04	2.0079+00	1.0685+09	3.1690+05

Fig. 9 - Output Data: Shock Layer Thermodynamic and Transport Variables

SHOCK LAYER CHEMICAL SPECIES SUMMARY

MOLECULAR SPECIES (PARTICLES/CM3)

ETA	Y/D	C2H	C3H	C4H	HCN	C2H2	C3	C2	H2	N2	O2	CO	CN
0.00	0.00	0.00	0.00	0.00	0.00	0.00	1.03+19	4.13+18	0.00	0.00	0.00	0.00	0.00
2.00-01	1.87-02	0.00	0.00	0.00	0.00	0.00	8.57+18	4.63+18	0.00	0.00	0.00	0.00	0.00
4.00-01	3.90-02	4.34+14	5.01+14	1.29+15	0.00	6.14+08	7.29+16	5.15+18	5.94+08	0.00	0.00	0.00	0.00
5.00-01	5.00-02	1.34+15	1.32+15	3.05+15	0.00	5.82+09	6.07+16	5.43+18	7.20+09	0.00	0.00	0.00	0.00
6.00-01	6.22-02	4.37+15	3.27+15	6.12+15	0.00	6.31+10	4.27+16	5.83+18	1.22+11	0.00	0.00	0.00	0.00
7.00-01	7.65-02	1.33+16	6.66+15	8.86+15	0.00	7.02+11	2.14+16	5.45+18	2.72+12	0.00	0.00	0.00	0.00
7.50-01	8.49-02	2.24+16	8.51+15	9.21+15	0.00	2.33+12	1.34+16	4.89+18	1.42+13	0.00	0.00	0.00	0.00
8.00-01	9.45-02	3.40+16	9.62+15	7.70+15	0.00	9.06+12	6.59+17	3.95+18	9.17+13	0.00	0.00	0.00	0.00
8.20-01	9.87-02	5.20+16	1.31+16	9.90+15	0.00	1.79+13	5.75+17	3.75+18	2.26+14	0.00	0.00	0.00	0.00
8.40-01	1.03-01	6.15+16	1.24+16	7.82+15	0.00	3.10+13	3.69+17	3.16+18	5.79+14	0.00	0.00	0.00	0.00
8.60-01	1.08-01	3.47+16	3.70+15	1.32+15	0.00	1.94+13	8.59+16	1.80+18	1.16+15	0.00	0.00	0.00	0.00
8.70-01	1.11-01	3.60+16	3.23+15	9.91+14	0.00	2.59+13	5.61+16	1.49+18	2.12+15	0.00	0.00	0.00	0.00
8.80-01	1.15-01	0.00	0.00	0.00	0.00	0.00	0.00	2.61+17	0.00	0.00	0.00	0.00	0.00
8.90-01	1.20-01	0.00	0.00	0.00	0.00	0.00	0.00	2.34+16	0.00	0.00	0.00	0.00	0.00
9.00-01	1.28-01	0.00	0.00	0.00	0.00	0.00	0.00	2.12+15	0.00	0.00	0.00	0.00	0.00
9.05-01	1.35-01	0.00	0.00	0.00	0.00	0.00	0.00	3.80+14	0.00	0.00	0.00	0.00	0.00
9.10-01	1.51-01	0.00	0.00	0.00	0.00	0.00	0.00	3.96+12	0.00	0.00	0.00	0.00	0.00
9.20-01	2.17-01	0.00	0.00	0.00	0.00	0.00	0.00	7.07+02	0.00	0.00	0.00	0.00	0.00
9.30-01	3.09-01	0.00	0.00	0.00	0.00	0.00	0.00	0.00	0.00	0.00	0.00	0.00	0.00
9.40-01	4.03-01	0.00	0.00	0.00	0.00	0.00	0.00	0.00	0.00	0.00	0.00	0.00	0.00
9.50-01	5.00-01	0.00	0.00	0.00	0.00	0.00	0.00	0.00	0.00	0.00	0.00	0.00	0.00
9.60-01	5.98-01	0.00	0.00	0.00	0.00	0.00	0.00	0.00	0.00	0.00	0.00	0.00	0.00
9.70-01	6.97-01	0.00	0.00	0.00	0.00	0.00	0.00	0.00	0.00	0.00	0.00	0.00	0.00
9.80-01	7.97-01	0.00	0.00	0.00	0.00	0.00	0.00	0.00	0.00	0.00	0.00	0.00	0.00
9.90-01	8.98-01	0.00	0.00	0.00	0.00	0.00	0.00	0.00	0.00	0.00	0.00	0.00	0.00
9.95-01	9.49-01	0.00	0.00	0.00	0.00	0.00	0.00	0.00	0.00	0.00	0.00	0.00	0.00
1.00+00	1.00+00	0.00	0.00	0.00	0.00	0.00	0.00	0.00	0.00	0.00	0.00	0.00	0.00

Fig. 10 - Output Data: Shock Layer Polyatomic and Diatomic Species

SHOCK LAYER CHEMICAL SPECIES SUMMARY

ATOMIC SPECIES (PARTICLES/CM3)

ETA	Y/D		C	N	O	HE	H+	C+	N+	C+	HE+		E-
0.00	0.00	0.00	1.60+18	0.00	0.00	0.00	0.00	0.00	0.00	0.00	0.00	0.00	0.00
2.00-01	1.87-02	0.00	2.07+18	0.00	0.00	0.00	0.00	0.00	0.00	0.00	0.00	0.00	0.00
4.00-01	3.90-02	1.57+14	2.77+18	0.00	0.00	0.00	0.00	0.00	0.00	0.00	0.00	0.00	0.00
5.00-01	5.00-02	6.15+14	3.38+18	0.00	0.00	5.56+14	0.00	0.00	0.00	0.00	0.00	0.00	0.00
6.00-01	6.22-02	3.11+15	4.20+18	0.00	0.00	1.48+15	0.00	0.00	0.00	0.00	0.00	0.00	0.00
7.00-01	7.65-02	1.89+16	5.93+18	0.00	0.00	4.19+15	0.00	0.00	0.00	0.00	0.00	0.00	0.00
7.50-01	8.49-02	4.93+16	6.89+18	0.00	0.00	7.85+15	0.00	0.00	0.00	0.00	0.00	0.00	0.00
8.00-01	9.48-02	1.47+17	7.91+18	0.00	0.00	1.76+16	0.00	0.00	0.00	0.00	0.00	0.00	0.00
8.20-01	9.87-02	2.38+17	8.30+18	0.00	0.00	2.75+16	0.00	0.00	0.00	0.00	0.00	0.00	0.00
8.40-01	1.03-01	4.13+17	8.35+18	0.00	0.00	4.35+16	0.00	0.00	0.00	0.00	0.00	0.00	0.00
8.60-01	1.08-01	7.34+17	8.96+18	0.00	0.00	6.82+16	0.00	0.00	0.00	0.00	0.00	0.00	0.00
8.70-01	1.11-01	1.04+18	8.80+18	0.00	0.00	9.55+16	0.00	0.00	0.00	0.00	0.00	0.00	0.00
8.80-01	1.15-01	1.33+18	8.07+18	0.00	0.00	1.17+17	4.63+13	1.76+16	0.00	0.00	4.98+05	1.15+13	1.76+16
8.90-01	1.20-01	1.70+18	5.63+18	0.00	0.00	1.67+17	1.21+15	8.33+16	0.00	0.00	3.26+06	8.25+13	8.95+16
9.00-01	1.23-01	2.92+18	2.89+18	0.00	0.00	2.58+17	1.91+16	2.33+17	0.00	0.00	5.72+10	1.69+14	2.55+17
9.05-01	1.33-01	3.59+18	1.52+18	0.00	0.00	3.21+17	6.42+16	2.98+17	0.00	0.00	4.56+11	2.73+14	3.22+17
9.10-01	1.51-01	3.96+18	2.42+17	0.00	0.00	3.29+17	3.91+17	1.76+17	0.00	0.00	1.68+13	3.43+14	5.67+17
9.20-01	2.17-01	2.95+18	3.87+12	0.00	0.00	3.21+17	7.04+17	5.08+12	0.00	0.00	7.58+13	3.74+14	7.04+17
9.30-01	3.09-01	2.72+18	0.00	0.00	0.00	3.07+17	7.71+17	0.00	0.00	0.00	1.34+14	3.61+14	7.69+17
9.40-01	4.03-01	2.62+18	0.00	0.00	0.00	3.03+17	8.01+17	0.00	0.00	0.00	1.20+14	3.54+14	8.01+17
9.50-01	5.00-01	2.54+18	0.00	0.00	0.00	2.95+17	8.20+17	0.00	0.00	0.00	1.35+14	3.49+14	8.20+17
9.60-01	5.98-01	2.46+18	0.00	0.00	0.00	2.91+17	8.40+17	0.00	0.00	0.00	1.50+14	3.43+14	8.40+17
9.70-01	6.97-01	2.42+18	0.00	0.00	0.00	2.88+17	8.61+17	0.00	0.00	0.00	1.59+14	3.39+14	8.61+17
9.80-01	7.97-01	2.38+18	0.00	0.00	0.00	2.86+17	8.73+17	0.00	0.00	0.00	1.68+14	3.37+14	8.73+17
9.90-01	8.93-01	2.35+18	0.00	0.00	0.00	2.83+17	8.83+17	0.00	0.00	0.00	1.76+14	3.34+14	8.83+17
9.95-01	9.49-01	2.31+18	0.00	0.00	0.00	2.81+17	8.94+17	0.00	0.00	0.00	1.85+14	3.31+14	8.94+17
1.00+00	1.00+00	2.28+18	0.00	0.00	0.00	2.79+17	9.05+17	0.00	0.00	0.00	1.94+14	3.28+14	9.05+17

Fig. 11 - Output Data: Shock Layer Atomic Species

FLUX USING LAST CALCULATED ENTHALPY PROFILE

ETA		T (DEG,K)	RHO (GM/CM3)	MU (GM/CM-SEC)	R (GM2/CM4-SEC)	CPR (ERGS/GM-DEG,K)	SKN (ERGS/CM-SEC-DEG,K)	PR	AB	G
.00	1	4,5000+03	8,1444-04	1,2358-03	1,0064-06	1,0529+08	2,9636+05	4,4570-01	3,0551+01	-2,8275-03
.20	1	4,6020+03	7,5738-04	1,2634-03	9,6910-07	1,2438+08	3,4985+05	4,5425-01	2,9427+01	-1,3521-03
.40	1	4,7458+03	6,9914-04	1,3034-03	9,1120-07	1,5131+08	4,1611+05	4,7576-01	2,7659+01	1,0991-03
.50	1	4,8489+03	6,6035-04	1,3332-03	8,8032-07	1,7157+08	4,6317+05	4,9332-01	2,6267+01	3,1643-03
.60	1	4,9962+03	6,1613-04	1,3781-03	8,4037-07	2,0023+08	5,2032+05	5,1023-01	2,4213+01	6,6057-03
.70	1	5,2664+03	5,4370-04	1,4649-03	7,8332-07	2,5245+08	6,3530+05	5,4070-01	2,1235+01	1,2709-02
.75	1	5,4394+03	5,0383-04	1,5116-03	7,5406-07	2,8429+08	7,1176+05	5,6237-01	1,9216+01	1,7526-02
.80	1	5,6972+03	4,5245-04	1,6002-03	7,1400-07	3,3564+08	8,4306+05	7,6395-01	1,6739+01	2,4479-02
.82	1	5,8482+03	4,1982-04	1,6521-03	6,9277-07	3,8522+08	9,7227+05	8,2184-01	1,5577+01	2,8537-02
.84	1	6,0770+03	3,8026-04	1,7282-03	6,8433-07	4,4946+08	2,0638+06	9,0174-01	1,4197+01	3,5443-02
.86	1	6,6459+03	2,8145-04	1,9028-03	4,2138-07	7,6721+07	1,4563+05	1,0029+00	1,2305+01	4,2255-02
.87	2	7,7499+03	1,7370-04	2,0631-03	3,5642-07	3,5993+07	8,4164+04	8,7827-01	1,1221+01	5,0153-02
.88	2	9,6463+03	1,2795-04	2,0160-03	2,5774-07	4,0932+07	9,5773+04	6,4251-01	1,1238+01	6,2045-02
.89	2	1,1150+04	9,4018-05	1,7088-03	1,6069-07	3,4759+07	1,3147+05	3,4154-01	8,7383+00	7,9667-02
.90	2	1,1793+04	6,2739-05	1,4734-03	9,2511-08	9,5754+07	1,7516+05	3,0208-01	6,1753+00	1,1243-01
.91	2	1,1924+04	4,3445-05	1,3620-03	5,6767-08	1,2782+08	2,1515+05	6,0344-01	4,3202+00	1,5413-01
.91	2	1,4222+04	1,6989-05	9,0219-04	1,5265-08	3,9938+08	2,9047+05	1,2411+00	2,0047+00	3,9243-01
.92	2	1,5529+04	5,1676-06	6,8759-04	5,6182-09	9,1317+08	3,2624+05	1,9262+00	1,4572+00	8,4007-01
.93	2	1,5979+04	7,7226-06	6,4542-04	4,9843-09	9,8657+08	3,2270+05	1,9728+00	1,0206+00	9,0613-01
.94	2	1,6118+04	7,5885-06	6,3293-04	4,8039-09	1,0076+09	3,2145+05	1,9835+00	1,0196+00	9,3036-01
.95	2	1,6225+04	7,4864-06	6,2350-04	4,6678-09	1,0233+09	3,2042+05	1,9918+00	1,0126+00	9,4462-01
.96	2	1,6307+04	7,4094-06	6,1644-04	4,5674-09	1,0349+09	3,1960+05	1,9957+00	1,0072+00	9,5922-01
.97	2	1,6372+04	7,3443-06	6,1065-04	4,4867-09	1,0441+09	3,1892+05	1,9994+00	1,0029+00	9,6956-01
.98	2	1,6427+04	7,2976-06	6,0624-04	4,4241-09	1,0515+09	3,1834+05	2,0022+00	9,9929-01	9,7838-01
.99	2	1,6427+04	7,2976-06	6,0624-04	4,4241-09	1,0515+09	3,1834+05	2,0022+00	9,9929-01	9,8669-01
.99	2	1,6505+04	7,2247-06	5,9965-04	4,3323-09	1,0621+09	3,1746+05	2,0059+00	9,9406-01	9,9217-01
1.00	2	1,6505+04	7,2247-06	5,9965-04	4,3323-09	1,0621+09	3,1746+05	2,0059+00	9,9406-01	1,0000+00

DELTA= 1,1690895+00 CM

CONTINUUM FLUX = 2,4357+04
LINE FLUX = 6,2200+03

Fig. 12 - Output Data: Final Temperature/Enthalpy Profile and Resultant Surface Flux

5. PRACTICAL ADVICE TO THE USER

Set forth in this section are some practical guides to using the VISC code as deduced by the author as a result of many attempts (successful and unsuccessful) at obtaining heating predictions.

The fundamental problem is prescribing a set of initial profiles (velocity, blown gas mass fraction, enthalpy) in a nonphysical coordinate which are sufficiently close to reality to get underway with a series of iterations. For a nonblowing problem this is not difficult at all. The boundary conditions on the velocity profile are $f = 0$ at the wall and $f = 1.0$ at the shock. A linear rise from the wall value to a level $f = 0.4$ at the edge of the boundary layer is reasonable. The edge of the boundary can be estimated as η (edge) $\sim 100/(Re_s)^{\frac{1}{2}}$. From the edge of the boundary layer to the shock, another linear profile is reasonable. Thus an input velocity profile might look like that sketched below.

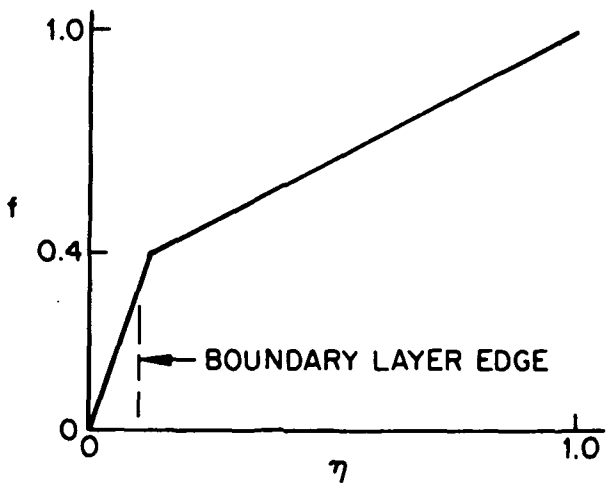

The boundary conditions on the enthalpy profile are $g = g_{wall}$ at the wall and $g = 1.0$ at the shock. The wall enthalpy can be prescribed directly or, if the usual wall temperature option is being used, the wall enthalpy can be estimated. The first iteration will correct any error in the wall enthalpy estimate. Again, a linear rise across the boundary layer region to the edge value is an adequate initial guess. The appropriate edge value will depend on the degree of radiative cooling. However, the edge value will typically be around $g_{edge} \sim 0.8$ to 0.9. It is normally best to err on the low side. A linear variation from boundary layer edge value to unity (the value at the shock) should be adequate to complete the initial enthalpy profile guess. Thus an input enthalpy profile might look like that sketched below.

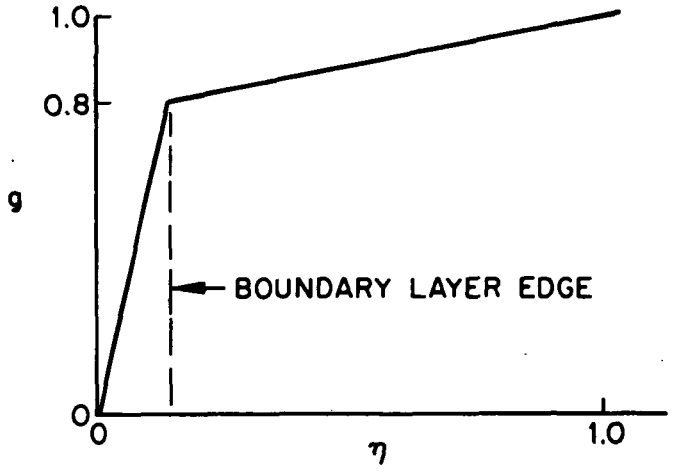

For a blowing problem, the selection of reasonable initial profiles is much more difficult. The user must first arrive at a reasonable blowing rate keeping in mind that the blowing rate will be fixed during a given computer "run." In previous years we were content to consider the blowing rate as an independent parameter.[6,7] In our recent studies of the Jovian entry heating problem,[8] a strong attempt has been made to determine the blowing rate based on the wall radiative flux and an effective energy of ablation. A conservative estimate to the wall flux will be the value deduced from a nonblowing calculation. A correlation of the reduction in the radiative flux

due to blowing (e.g., the correlation presented by Page[10]) can be used to obtain a much closer estimate of the "final" blowing rate.

Having fixed upon a blowing rate, the user next must decide on an approximate location of the extent of the blown gas layer, i.e., the value of the η coordinate where the stream function is zero, $\eta = \eta^*$. The shear layer with its rapid change in velocity, blown gas mass fraction and enthalpy will be centered (approximately) at this blown gas-atmospheric gas interface. The author can offer no general rule for determining the value of η^*. It will be necessary for the user to experiment with the problem at hand to obtain a feeling for the interface location. A single pass through the entire iterative cycle or even a single iterative solution to the momentum equation will provide a good second estimate for the value of η^*. This is true even if the initial guess for the profiles is so poor as to cause the VISC to undergo an error termination in the radiative transfer or energy equation routines. The user should call for the diagnostic output and determine from the output the value of the η coordinate where the stream function (identified as PSI) passes through zero.

Assume, then, that the user is unable to arrive at an a priori estimate for the interface location $\eta = \eta^*$. A practical approach might be to set $\eta^* = 0.5$ and select initial velocity, blown gas mass fraction and enthalpy profiles around that value. Typically, the velocity function f increases linearly from the wall value $f = 0$ to the level $f = 0.1$ at the inner edge of the shear layer. As in the nonblowing problem, the velocity at the outer edge of the shear layer is $f = 0.4$ and the velocity increases in a nearly linear fashion to its shock value $f = 1.0$. The extent of the shear layer is (as for the nonblowing case) on the order of $100/(Re_s)^{\frac{1}{2}}$. A simple straight line interpolation between the value at the inner and outer edge completes the initial velocity profile guess. A typical guess for the velocity profile based on $\eta^* = 0.5$ is shown in Fig. 13.

The blown gas mass fraction can be taken as a constant value of unity (the wall value) out to the inner edge of the shear layer. The blown gas mass fraction can be assumed to drop in a linear manner to a value of zero

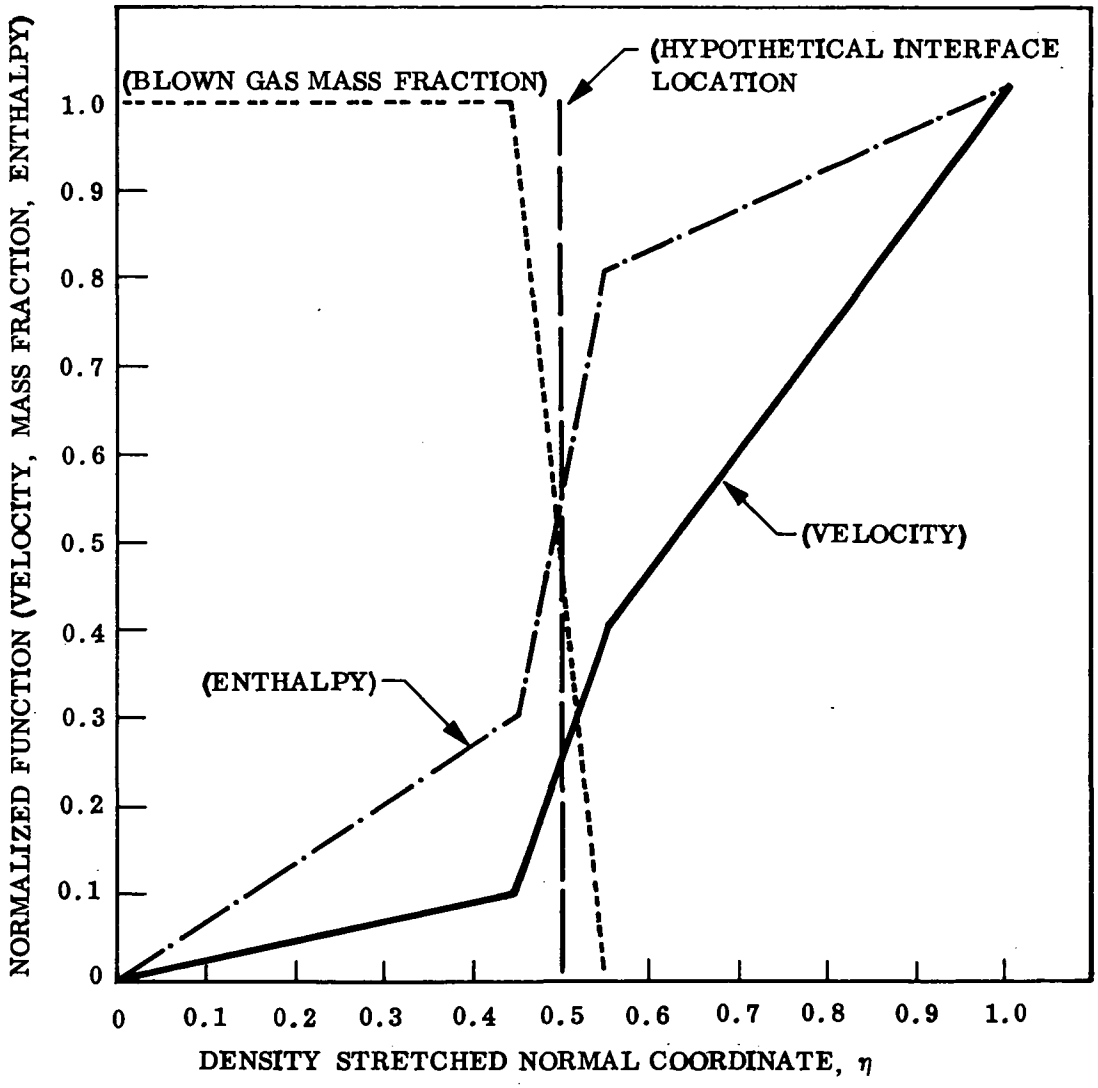

Fig. 13 - Representative Profiles of Velocity, Mass Fraction and Enthalpy for a Massive Blowing Problem

(the shock value) as the outer edge of the shear layer. Such a guess for the blown gas mass fraction is shown in Fig. 13.

No general rules can be given for selection of the initial enthalpy profile. A crude estimate is to assume that the enthalpy is constant at the wall value out to the inner edge of the shear layer and then rises linearly across the shear layer (as in the nonblowing case described above) to a value on the order of 0.8 to 0.9 at the outer edge of the shear layer. Again, a linear variation for outer shear layer edge to the shock value of unity completes the enthalpy guess. The enthalpy profile estimate using this approach is shown in Fig. 14. Under conditions of massive blowing and strong radiative coupling, the blown gas will experience a substantial rise in enthalpy before it reaches the interface. If the user initiates the solution with a constant enthalpy in the blown gas layer, it will probably be necessary to perform a number of single iteration runs observing the inward movement of the region heated blown gas before a reasonably consistent enthalpy profile would be achieved.

The mesh selection remains to be discussed. The VISC code does not provide an automated routine for selection of points in the η coordinate system. The user should provide for the location of a few mesh points within the shear layer region. It is not at all necessary nor practical to provide a fine mesh inside the shear layer when the Reynolds number becomes large, say $Re_s \sim 10^6$. The user must judiciously select the remaining points to provide resolution of the region near the shockwave where the radiative cooling produces a substantial drop in enthalpy and in other regions (particularly in the blown gas layer) where the radiative flux divergence changes rapidly. Normally the spatial resolution around the interface is dominated by requirements to capture the peak in absorption of the intense incoming radiative flux.

The selection of the points at which the flux divergence is calculated (the Q-POINT distribution shown in Fig. 3) reflects the comments given above concerning the need to obtain an accurate accounting of the rapid change in flux divergence which occurs in various regions near the edge and interior to the blown gas layer. An η point and its designation as a Q-POINT is required

very near the shock, e.g., at $\eta = .99$ or $\eta = .995$. This requirement stems from the fact that the flux divergence due to atomic lines changes by at least one order as the calculation moves from a point exactly on the (discontinuous) shockwave to a point which is a minute physical distance inside the shock layer.[7] To avoid the requirement of a detailed resolution of the line flux divergence near the shock, the code uses the flux divergence from the point nearest the shock to provide an extrapolated value at the shock. For this reason, a point reasonably close to the shock corresponding to a physical distance of about 1% of the shock layer thickness) is required.

At what point does the heating prediction obtained by the VISC code constitute a "solution" to a particular entry problem? This question is at the heart of the convergence difficulties. For nonblowing problems the author has normally set a convergence level of 5% with the realization that the precision in the radiative and convective flux calculation will be at least that good. For a blowing problem the author has worked toward a goal of a 10% level of precision. By this is meant the following. Let the radiative flux at some cycle be the i^{th} value. Then, if the computation were continued an endless number of iterations, the asymptotically approached radiative heating value would be within 10% of the i^{th} value. The degree of precision is measured by comparing the radiative flux from the guessed and calculated enthalpy. The user is warned, however, that in order for the above measured precision to be valid the enthalpy profile must be converged to about 10% at <u>most</u> points across the shock layer. The exception is the few points in the shear layer region where large spatial variations occur: In the final analysis it is the responsibility of the user to interpret the results of the VISC code in an intelligent way.

6. REFERENCES

1. K. H. Wilson and H. Hoshizaki, "Inviscid, Nonadiabatic Flow About Blunt Bodies," AIAA J., Vol. 3, pp. 67-74, 1965.

2. H. Hoshizaki and K. H. Wilson, "Viscous, Radiating Shock Layer About a Blunt Body," AIAA J., Vol. 3, pp. 1614-1622, 1965.

3. H. Hoshizaki and K. H. Wilson, "Convective and Radiative Heat Transfer During Superorbital Entry," AIAA J., Vol. 5, pp. 25-35, 1967.

4. H. Hoshizaki and L. E. Lasher, "Convective and Radiative Heat Transfer to an Ablating Body," AIAA J., Vol. 6, pp. 1441-1449, 1968.

5. K. H. Wilson and R. Greif, "Radiation Transport in Atomic Plasmas," J.Q.S.R.T., Vol. 8, pp. 1061-1086, 1968.

6. K. H. Wilson, "Massive Blowing Effects on Viscous, Radiating, Stagnation-Point Flow," AIAA Paper No. 70-203, AIAA 8th Aerospace Sciences Meeting, New York, Jan. 19-21, 1970.

7. K. H. Wilson, "Stagnation Point Analysis of Coupled Viscous Radiating Flow with Massive Blowing," NASA CR-1548, June 1970.

8. K. H. Wilson, "Recent Studies of the Effects of Massive Blowing on Planetary Entry Heating," LMSC 4-05-71-8, Jan. 1971.

9. Y. S. Chou, "Locally Nonsimilar Solutions for Radiating Shock Layers About Smooth Axisymmetric Bodies," NASA CR-1989, Mar., 1972.

10. W. A. Page, "Aerodynamic Heating for Probe Vehicles Entering the Outer Planets," Preprint No. AAS-71-144, presented at the American Astronautical Society Meeting, Seattle, Washington, June 28-30, 1971.

NASA-Langley, 1973 —— 33